Dynamic Contrast-Enhanced MRI of the Patellar Bone: How to Quantify Perfusion

Dirk H.J. Poot, PhD,[1,2]* Rianne A. van der Heijden, MD, PhD,[3,4] Marienke van Middelkoop, PhD,[4] Edwin H.G. Oei, MD, PhD,[3] and Stefan Klein, PhD[1]

Purpose: To identify the optimal combination of pharmacokinetic model and arterial input function (AIF) for quantitative analysis of blood perfusion in the patellar bone using dynamic contrast-enhanced magnetic resonance imaging (DCE-MRI).
Materials and Methods: This method design study used a random subset of five control subjects from an Institutional Review Board (IRB)-approved case–control study into patellofemoral pain, scanned on a 3T MR system with a contrast-enhanced time-resolved imaging of contrast kinetics (TRICKS) sequence. We systematically investigated the reproducibility of pharmacokinetic parameters for all combinations of Orton and Parker AIF models with Tofts, Extended Tofts (ETofts), and Brix pharmacokinetic models. Furthermore, we evaluated if the AIF should use literature parameters, be subject-specific, or group-specific. Model selection was based on the goodness-of-fit and the coefficient of variation of the pharmacokinetic parameters inside the patella. This extends previous studies that were not focused on the patella and did not evaluate as many combinations of arterial and pharmacokinetic models.
Results: The vascular component in the ETofts model could not reliably be recovered (coefficient of variation [CV] of v_p >50%) and the Brix model parameters showed high variability of up to 20% for k_{el} across good AIF models. Compared to group-specific AIF, the subject-specific AIF's mostly had higher residual. The best reproducibility and goodness-of-fit were obtained by combining Tofts' pharmacokinetic model with the group-specific Parker AIF.
Conclusion: We identified several good combinations of pharmacokinetic models and AIF for quantitative analysis of perfusion in the patellar bone. The recommended combination is Tofts pharmacokinetic model combined with a group-specific Parker AIF model.
Level of Evidence: 2
Technical Efficacy: Stage 1

J. MAGN. RESON. IMAGING 2018;47:848–858.

Research suggests that altered blood perfusion of the patellar bone may play a role in the pathogenesis of patellofemoral pain (PFP), a common knee complaint.[1–8] Blood perfusion can be visualized and analyzed quantitatively using dynamic contrast-enhanced magnetic resonance imaging (DCE-MRI).[9] Despite the well-described use of DCE-MRI for a variety of indications such as tumors and cerebral strokes,[10,11] only a limited number of publications address DCE-MRI in bone,[12–16] and none specifically in the patella. DCE-MRI in bone has been limited due to the sparse vascularization of bone and the typical low contrast enhancement compared to surrounding tissues.[12,16] The mobility of the patella poses an additional specific challenge.

Signal intensity changes in the DCE-MRI time series are due to the contrast medium entering the tissue through feeding arteries, residing in the extravascular space, and subsequent draining. This process can be studied semiquantitatively using measures like time-to-peak, or quantitatively by fitting a pharmacokinetic model to the DCE-MRI data to extract truly quantitative measures of perfusion.[9] Quantitative DCE-MRI requires choosing one of multiple proposed arterial input functions (AIFs) and one of the pharmacokinetic

View this article online at wileyonlinelibrary.com. DOI: 10.1002/jmri.25817

Received Mar 17, 2017, Accepted for publication Jun 29, 2017.

*Address reprint requests to: D.H.J.P., Erasmus MC, Na2516, Depts. of Medical Informatics & Radiology, Biomedical Imaging Group Rotterdam, P.O. Box 2040, 3000 CA Rotterdam, The Netherlands. E-mail: d.poot@erasmusmc.nl

From the [1]Biomedical Imaging Group Rotterdam, Departments of Medical Informatics & Radiology, Erasmus MC, Rotterdam, The Netherlands; [2]Quantitative Imaging, Department of Imaging Physics, Delft University of Technology, Delft, The Netherlands; [3]Department of Radiology & Nuclear Medicine, Erasmus MC, Rotterdam, The Netherlands; and [4]Department of General Practice, Erasmus MC, Rotterdam, The Netherlands

Additional supporting information may be found in the online version of this article.

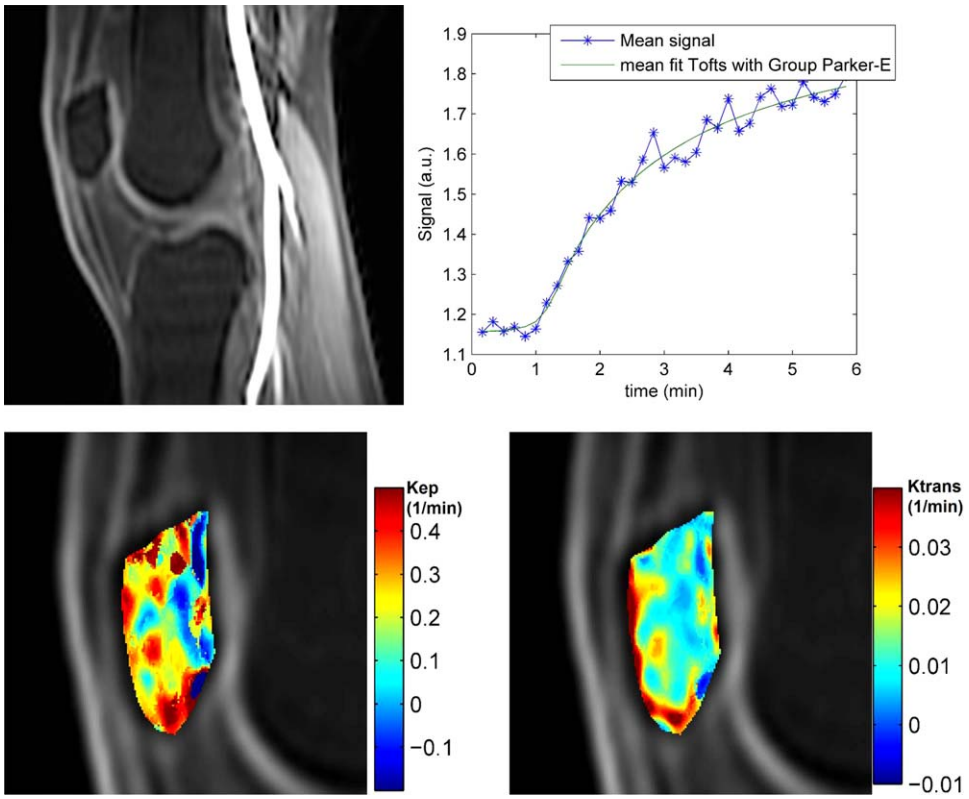

FIGURE 1: Example DCE image at maximum arterial enhancement in one of the control subjects, time intensity curve, and fit with Tofts' model, including the overlays showing the apparent heterogeneity inside the patella.

models that together are able to describe the dynamic contrast concentration. Selection of appropriate models is especially relevant for low signal intensity regions since a too complex model (too many degrees of freedom) will be influenced stronger by acquisition noise and, hence, is less sensitive to between-group or between-subject differences in perfusion. Moreover, a model that cannot describe the DCE-MRI signal with sufficient accuracy may fail to detect relevant changes in perfusion. Although quantitative DCE-MRI has been performed in several bones,[9] no thorough evaluation of the optimal combination of AIF and a pharmacokinetic model has been presented. Due to the differences in perfusion, the model evaluation results obtained on tumor tissue are not directly applicable to the analysis of patellar perfusion.[17]

The aim of this study was to identify the optimal combination of pharmacokinetic model and AIF for quantitative analysis of perfusion in the patellar bone using DCE-MRI. As potentially appropriate AIF models we selected three models by Orton et al[18] and several parametrizations of Parker et al's model.[19] As pharmacokinetic models we selected the models of Brix, Tofts, and the extended model of Tofts.[20]

Materials and Methods

DCE-MRI Acquisition

This method design study used a random subset of five control subjects and five patients from an Institutional Review Board (IRB)-approved case–control study into patellofemoral pain containing 134 subjects.[21] All subjects provided written informed consent. A 3T MRI scanner (Discovery MR750, GE Healthcare, Milwaukee, WI) with a dedicated 8-channel knee coil (Invivo, Gainesville, FL) was used.

DCE-MRI was acquired by a time-resolved imaging of contrast kinetics (TRICKS) sequence with anterior–posterior (AP) frequency encoding direction to avoid pulsation artifacts of the popliteal artery into the region of interest. MRI parameters were: in-plane pixel resolution 1.5 mm, slice thickness 5 mm, field of view 380 × 380 × 70 mm, acquisition matrix 256 × 128, 14 sagittal slices, 70% sampling in the phase direction, echo time (TE) = 1.7 msec, repetition time (TR) = 9.3 msec, flip angle (FA) = 30°. The DCE-MRI protocol consisted of 35 phases of 10.30 ± 0.07 sec (constant within subject). Intravenous contrast administration of 0.2 mmol/kg gadopentetate dimeglumine (Magnevist, Bayer, Berlin, Germany), at a rate of 2 ml/s, was started after the first phase. Additionally, a nonfat-suppressed 3D SPGR sequence with in-plane resolution of 0.3 × 0.3 mm and 0.5 mm slices was acquired before contrast administration for delineation of the patellar bone marrow. See Figs. 1 and 2 for an example image of a control subject and a patient, respectively.

Motion Compensation

Image-driven motion compensation was applied, based on a technique developed for T_1 mapping in femoral and tibial articular cartilage.[22] A registration mask was drawn around the patella in the 3D SPGR image. Within this mask the DCE-MRI time series were automatically registered to the first DCE-MRI timepoint

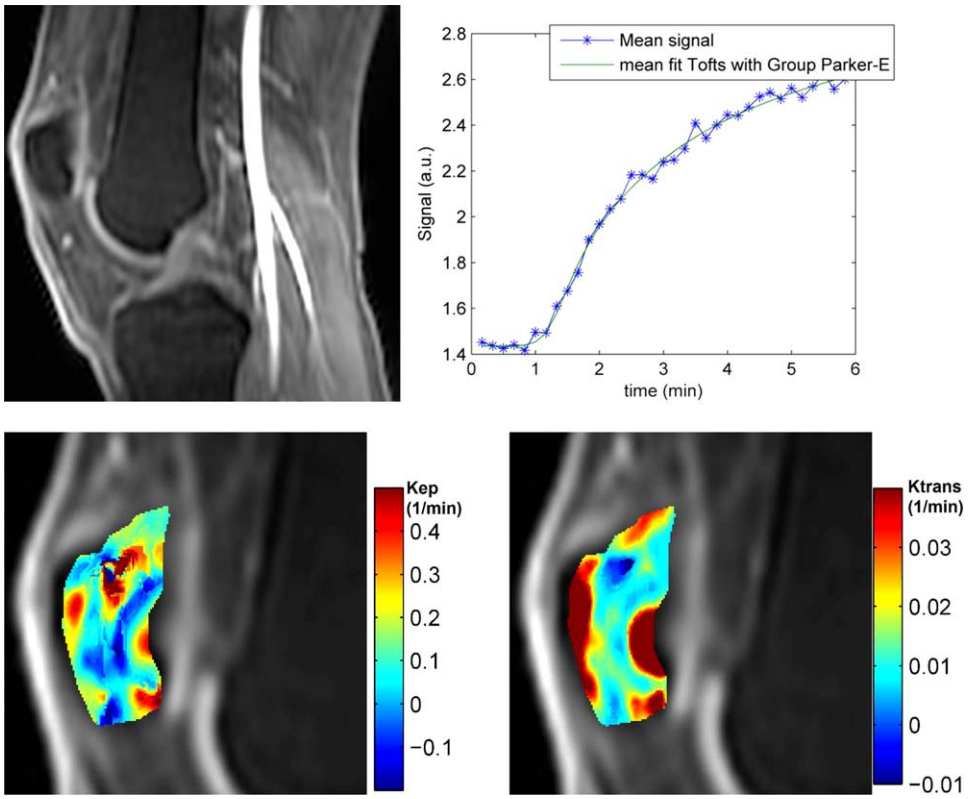

FIGURE 2: Example DCE image at maximum arterial enhancement in one of the patients, time intensity curve, and fit with Tofts' model, including the overlays showing the apparent heterogeneity inside the patella.

using a rigid transformation model. Subsequently, the first phase was registered to the 3D SPGR image and all DCE-MRI scans were transformed to the grid of the high-resolution 3D SPGR. Visual inspection indicated successful alignment of the time series.

Quantitative DCE-MRI Modeling

The dynamic DCE-MRI signal in each voxel $A(t)$ is described by a combination of three models: The *AIF,* the pharmacokinetic response function (P), and the function that relates contrast concentration to signal intensity (S), combined as:

$$A(t) = S_\xi\left((AIF_\chi * P_\phi)(t)\right) \quad (1)$$

where $*$ denotes convolution and ξ,χ,φ are model parameters.

For the *AIF* model we evaluated three computationally efficient models of Orton et al[18] (Orton1, Orton2, Orton3), five variations on Parker et al's model[19] with increasing degrees of freedom (Parker-L, Parker-A, Parker-S, Parker-E, Parker-T), as well as a "dummy" triangle-shaped AIF function. The *AIF* parameters χ were estimated from a manually outlined arterial region, either from a single subject (*subject-specific*) or from the entire group of subjects (*group-specific*), or obtained from the literature (*literature-based*).

For the pharmacokinetic model P we evaluate Brix, Tofts, and Extended Tofts (ETofts) models.[20,23] The Brix model has *AH,* k_{ep}, and k_{el} as parameters φ, while Tofts model has K_{trans} and k_{ep} as φ, and ETofts adds v_p to it; each model additionally includes a delay parameter.

For S we used a standard model suitable for the SPGR based sequence with one free parameter $\xi = S_0$.

The Supplementary Material sections S.1–S.3 provide more details on the models and section S.4 provides details on the maximum likelihood estimation method used to recover ξ, χ, and φ with constraints provided in Table 1.

Technical Validation on Phantom Data

To validate the model fitting method, a simulated dataset from a DCE-MRI anthropomorphic digital reference phantom was used.[24] This phantom, designed to validate fitting methods, contains a simulation of perfusion inside a brain tumor, which was selected as the volume-of-interest (VOI). All AIF models were fitted on selected arterial voxels and evaluated with the R-square value. Subsequently, these AIFs were used to analyze the provided VOI with ETofts. Accuracy of the pharmacokinetic parameters was measured by the median absolute difference (MAD) between the estimated and ground truth parameters of the ETofts model in the VOI and compared to the median ground truth value.

Comparative Evaluation of AIF Models

The AIF models were fitted to the voxels in a region of interest (ROI) drawn in the center of the popliteal artery, approximately at the level of the center of the patella. This artery was the largest artery in the field of view and could easily be identified in all subjects. Fit quality was evaluated by Akaike's information criterion (AIC)[25,26]:

TABLE 1. Parameters, Units, and Constraints Applied During Estimation

Model	All	Tofts and ETofts		ETofts	Brix		
parameter unit	delay min	K_{trans} $(min)^{-1}$	k_{ep} $(min)^{-1}$	v_p (fraction)	AH min^{-2}	k_{ep} $(min)^{-1}$	k_{el} $(min)^{-1}$
Lower bound optimization	0	-0.1	-1	-0.1	-0.2	-1	0
Lower bound initialization	0.17	-0.01	-0.2	-0.001	-0.05	-0.2	0.2
Upper bound initialization	2.50	0.5	0.5	0.001	0.25	0.8	4
Upper bound optimization	5	1	3	0.2	1	3	10

$$AIC = 2k + n\ln(SSR) \quad (2)$$

where k is the number of parameters in the model (for all subjects), n is the number of samples to which the model is fitted, and SSR is the sum of squared residuals (measurements minus values predicted by the fitted model). AIC provides an objective way to compare models with different complexities. Since the voxels from which the AIF is estimated are selected from a small region, they have substantial spatial correlation, which reduces the effective number of degrees of freedom. To avoid a biased model selection due to these correlations, we evaluated the AIC on one randomly selected voxel within the arterial ROI of each subject, and we report the mean and standard deviation of the AIC over 1000 random selections.

Comparative Evaluation of Pharmacokinetic Models

Each combination of AIF and pharmacokinetic model was fitted to the DCE-MRI data. For each pharmacokinetic parameter we computed its weighted mean over a VOI consisting of the patellar bone marrow, drawn by an experienced observer (R.H.). As weights we used $1/CRLB$ where $CRLB$ is the Cramér-Rao lower bound at each voxel, which is a measure of fit uncertainty (see Supporting Information S.4). In this way, we suppress the influence of voxels with an unreliable fit. The mean and coefficient of variation (CV = standard deviation / |mean|) across subjects were computed to investigate reproducibility. The residual ($=\sqrt{SSR}$) was computed to evaluate goodness-of-fit.

TABLE 2. Median Absolute Difference (MAD) of ETofts Parameters in the VOI of the Phantom Experiment for the Different AIF Models

	K_{trans} (1/min)	k_{ep} (1/min)	v_p (fraction)
Literature-based			
Triangle	0.1986	0.345	0.0155
Orton1	0.0696	0.459	0.0111
Orton2	0.0672	0.466	0.0059
Orton3	0.0081	0.446	0.0074
Parker	0.0133	0.468	0.0079
Subject-specific			
Triangle	0.5461	0.387	0.0379
Orton1	0.0696	0.459	0.0111
Orton2	0.0695	0.032	0.0126
Orton3	0.0293	0.043	0.0107
Parker-A	0.0118	0.082	0.0092
Parker-S	0.0059	0.070	0.0047
Parker-E	0.0096	0.085	0.0058
Parker-T	0.0079	0.086	0.0011
Median ground truth	0.0701	0.418	0.0138

Median ground truth values are given in the bottom row.

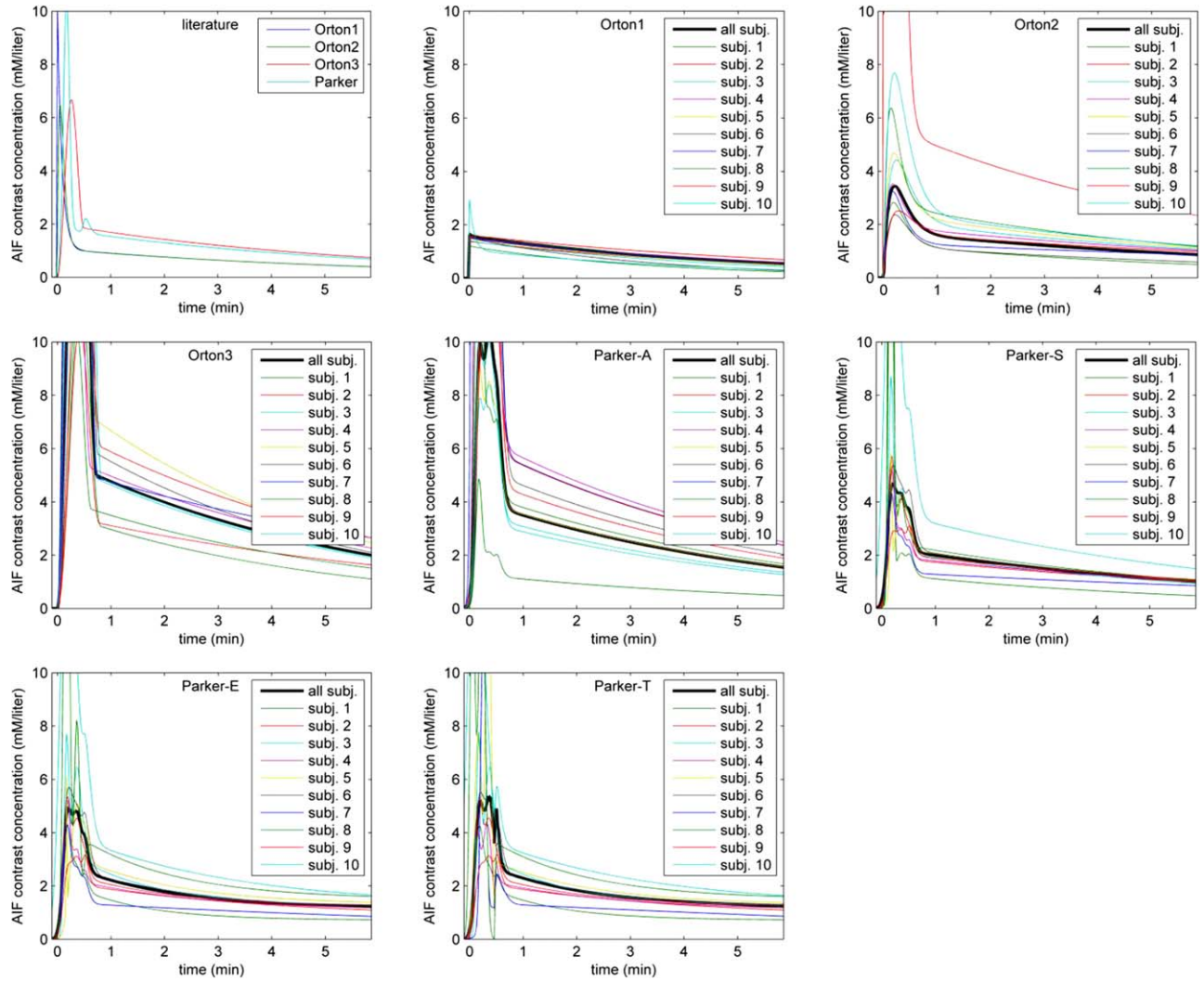

FIGURE 3: Literature-based, subject-specific, and group-specific arterial contrast concentration, from left to right, top to bottom: Literature, Orton1, Orton2, Orton3, Parker-A, Parker-S, Parker-E, Parker-T. In each figure, the group-specific estimate is shown by the black bold line.

TABLE 3. Mean (SD) of the AIC of AIF Fits

	Literature-based		Subject-specific		Group-specific	
Triangle	2636.0	(14.6)	1999.8	(14.2)	1987.9	(13.3)
Orton1	1906.7	(21.6)	1365.6	(12.3)	1346.9	(15.1)
Orton2	1963.2	(10.9)	560.8	(21.5)	751.8	(38.0)
Orton3	1308.5	(17.3)	605.9	(19.6)	793.5	(33.8)
Parker-L	1348.8	(16.1)				
Parker-A			576.6	(24.4)	756.1	(35.8)
Parker-S			454.4	(36.5)	725.4	(42.2)
Parker-E			244.7	(52.6)	662.0	(47.9)
Parker-T			297.3	(54.6)	640.2	(53.8)

Lower values indicate a better model fit.

TABLE 4. For Each AIF and Pharmacokinetic Model, the Mean Over the Five Control Subjects of Each Parameter and the Residual

	Tofts		Extended Tofts			Brix			Residual		
	K_{trans}	k_{ep}	K_{trans}	k_{ep}	v_p	AH	k_{ep}	k_{el}	Tofts	ETofts	Brix
Literature-based											
Triangle	0.057	−0.133	0.050	−0.139	0.000	0.127	0.023	0.464	0.119	0.119	0.070
Orton1	0.023	0.112	0.021	0.116	0.000	0.059	0.255	1.415	0.083	0.081	0.069
Orton2	0.025	0.123	0.021	0.125	0.000	0.062	0.284	1.407	0.081	0.081	0.069
Orton3	0.016	0.148	0.014	0.151	0.000	0.035	0.215	1.430	0.079	0.079	0.069
Parker	0.015	0.131	0.014	0.134	0.000	0.037	0.313	0.954	0.081	0.081	0.069
Subject-specific											
Triangle	0.770	−0.157	0.756	−0.163	0.050	0.924	0.009	0.249	0.146	0.147	0.114
Orton1	0.035	0.211	0.029	0.203	0.004	0.057	0.234	2.148	0.074	0.073	0.073
Orton2	0.014	0.106	0.013	0.041	0.000	0.029	0.246	1.594	0.084	0.074	0.070
Orton3	0.005	0.095	0.005	0.097	0.000	0.011	0.229	1.306	0.085	0.086	0.068
Parker-A	0.008	0.127	0.007	0.131	0.000	0.017	0.254	1.195	0.084	0.084	0.069
Parker-S	0.015	0.160	0.013	0.161	0.000	0.032	0.210	1.259	0.080	0.079	0.069
Parker-E	0.015	0.191	0.013	0.193	0.000	0.030	0.233	1.856	0.076	0.076	0.069
Parker-T	0.014	0.177	0.012	0.180	0.000	0.030	0.250	1.664	0.077	0.077	0.068
Group-specific											
Triangle	0.752	−0.139	0.734	−0.145	0.053	0.883	−0.056	0.488	0.132	0.132	0.105
Orton1	0.031	0.219	0.025	0.207	0.004	0.050	0.296	1.724	0.074	0.072	0.073
Orton2	0.020	0.212	0.017	0.213	0.000	0.041	0.302	1.589	0.075	0.075	0.069
Orton3	0.004	0.071	0.004	0.075	0.000	0.008	0.155	1.198	0.088	0.089	0.068
Parker-A	0.007	0.136	0.007	0.139	0.000	0.015	0.199	1.212	0.080	0.079	0.069
Parker-S	0.015	0.197	0.014	0.198	0.000	0.032	0.262	1.367	0.076	0.076	0.069
Parker-E	0.014	0.187	0.012	0.189	0.000	0.028	0.236	1.490	0.075	0.075	0.069
Parker-T	0.014	0.181	0.011	0.184	0.000	0.027	0.230	1.799	0.076	0.076	0.069

K_{trans}, k_{ep}, k_{el} in $1/min$; v_p is a fraction; AH is in $1/min^2$; residual norm is in arbitrary units but it can be compared across all model combinations.

RESULTS

Technical Validation on Phantom Data

On the phantom data, the Parker-T model fitted best to the arterial signal with an R-square value of 0.9994, whereas Parker-E and Orton3 had R-square of 0.9983 and 0.9876, respectively. Orton3 fitted best among the Orton models. See Table 2 for the MAD of K_{trans}, k_{ep}, and v_p inside the VOI. Parker-T had the lowest MAD for K_{trans} and v_p.

Comparative Evaluation of AIF Models

Figure 3 shows the AIFs that were estimated by the different models. There were substantial differences between AIFs when estimated for each subject individually, especially for the models Orton2, Orton3, and Parker-A. The substantial differences in contrast concentration in the tail of the curve were observed to be correlated to under/overestimation of the baseline signal intensity ξ. For subject-specific Parker-E and Parker-T, the first-pass contrast concentration differed substantially from the group-specific first-pass and the first-pass as provided by the literature-based AIFs. The group-specific Parker-T was also substantially different from the literature-based Parker model.

Table 3 shows the mean and standard deviation of the AIC value of the AIF fits over the 1000 random selections of one voxel per subject. Note that in Eq. (2), $n = 175$ (35 timepoints $\times$ 1 randomly selected voxel $\times$ 5 subjects) and k varies between 20 (literature-based AIF; only estimating delay and ξ per subject) and 123 (subject-specific Parker-T).

TABLE 5. For Each AIF and Each Parameter of the Pharmacokinetic Models, the CV (%) Over the Five Control Subjects

	Tofts		Extended Tofts			Brix			Residual		
	K_{trans}	k_{ep}	K_{trans}	k_{ep}	v_p	AH	k_{ep}	k_{el}	Tofts	ETofts	Brix
Literature-based											
Triangle	62.9	−31.4	70.0	−20.1	82.2	23.9	492.7	79.1	20.5	20.7	14.9
Orton1	35.5	27.3	52.4	26.5	−165.5	30.7	43.5	61.9	16.5	16.4	15.9
Orton2	35.6	24.5	48.7	23.2	436.8	35.7	61.0	60.8	15.9	16.5	15.8
Orton3	32.4	23.9	40.0	22.8	−249.6	32.8	28.4	50.0	15.9	16.2	16.2
Parker	36.8	24.0	45.4	23.9	188.0	31.5	41.7	73.9	16.2	16.4	16.1
Subject-specific											
Triangle	32.9	−16.4	34.5	−14.3	77.3	6.8	1120.1	127.8	25.4	25.2	23.4
Orton1	23.7	27.3	36.8	28.9	61.4	28.4	26.0	31.6	15.3	15.3	16.1
Orton2	57.1	223.2	53.3	950.9	636.6	60.5	32.4	47.7	35.7	15.9	16.1
Orton3	52.5	40.9	53.9	39.8	−514.8	45.6	76.9	44.3	16.6	17.0	16.7
Parker-A	53.2	53.1	46.1	50.1	249.9	58.8	51.5	51.8	18.6	19.7	16.2
Parker-S	53.8	79.3	52.9	79.3	3897.8	49.5	69.4	60.1	17.2	17.4	15.9
Parker-E	19.7	25.5	27.6	25.3	199.9	24.1	32.0	20.0	17.5	18.2	15.2
Parker-T	27.3	22.5	31.1	21.7	583.9	28.1	28.8	31.9	16.6	17.1	15.9
Group-specific											
Triangle	23.2	−18.8	25.5	−16.9	78.8	8.8	−108.3	43.3	24.7	24.4	22.6
Orton1	26.2	16.8	38.4	17.9	56.8	29.6	43.8	62.3	15.3	15.2	15.9
Orton2	27.6	20.2	43.3	19.3	−420.5	32.2	28.0	44.8	15.7	16.0	15.7
Orton3	33.8	56.3	40.4	53.0	335.0	29.3	43.1	46.7	18.4	18.8	16.5
Parker-A	34.3	28.7	40.4	28.2	497.9	31.7	34.2	48.5	16.6	17.0	16.5
Parker-S	28.8	21.1	38.8	20.1	−713.5	32.4	32.9	54.6	15.9	16.2	16.2
Parker-E	29.3	22.8	42.0	22.1	8001.0	32.4	25.6	45.3	15.3	15.7	15.4
Parker-T	29.3	23.3	44.2	22.7	−1748.7	32.1	27.8	19.8	15.4	15.9	15.5

The three right-most columns show the CV of the residual.

The AIC of Parker-E and Parker-T were much lower than the AIC of the Orton models. All models substantially improved over the triangle AIF.

Comparative Evaluation of Pharmacokinetic Models

Tables (4–7) show the mean and CV across control subjects and across patients of the pharmacokinetic parameters, as well as of the residual norm, for all combinations of AIF and pharmacokinetic models.

Variations in parameter values for different AIF models were observed, both for controls (Table 4) and patients (Table 6); eg, 20% difference in Brix k_{el} between group-specific Parker E&T. The residual of ETofts was not substantially lower than the residual of Tofts, which indicates that, in our patellar VOI, inclusion of the vascular component did not lead to a better fit. This is additionally reflected in that the vascular fraction v_p is close to zero. For most AIF models, the residual of the Brix model was ~10% lower than the residual of Tofts and ETofts. The residual norm did not vary substantially across AIF models, except for the "dummy" Triangle AIF and the literature-based AIFs combined with the ETofts model, which resulted in a higher residual norm.

Table 5 shows that for the control subjects the pharmacokinetic parameters estimated with subject-specific AIF models had an increased CV compared to pharmacokinetic parameters estimated with literature-based and group-specific AIF models. For most combinations there were only small differences in CV of the parameters between literature-based

TABLE 6. For Each AIF and Pharmacokinetic Model, the Mean Over the Five Patients of Each Parameter and the Residual

	Tofts		Extended Tofts			Brix			Residual		
	K_{trans}	k_{ep}	K_{trans}	k_{ep}	v_p	AH	k_{ep}	k_{el}	Tofts	ETofts	Brix
Literature-based											
Triangle	0.063	−0.159	0.050	−0.166	0.000	0.212	−0.034	0.803	0.163	0.161	0.091
Orton1	0.021	0.093	0.018	0.102	0.000	0.121	0.233	1.740	0.107	0.104	0.088
Orton2	0.023	0.109	0.020	0.114	0.000	0.138	0.171	2.095	0.105	0.103	0.089
Orton3	0.014	0.133	0.013	0.135	0.000	0.073	0.276	2.138	0.100	0.100	0.086
Parker	0.013	0.112	0.012	0.115	0.000	0.075	0.214	1.818	0.103	0.104	0.086
Subject-specific											
Triangle	0.652	−0.220	0.545	−0.227	0.081	0.874	−0.072	0.243	0.290	0.290	0.232
Orton1	0.030	0.207	0.024	0.193	0.007	0.290	0.215	2.132	0.101	0.097	0.106
Orton2	0.019	0.201	0.017	0.201	0.001	0.111	0.229	1.837	0.094	0.093	0.091
Orton3	0.004	0.037	0.003	0.035	0.000	0.017	0.098	1.607	0.127	0.126	0.085
Parker-A	0.003	0.039	0.003	−0.002	0.000	0.017	0.118	1.523	0.125	0.118	0.085
Parker-S	0.012	0.170	0.011	0.167	0.000	0.058	0.211	2.118	0.097	0.096	0.086
Parker-E	0.011	0.159	0.009	0.157	0.000	0.049	0.200	1.552	0.097	0.095	0.085
Parker-T	0.010	0.155	0.009	0.151	0.001	0.051	0.259	2.023	0.099	0.097	0.085
Group-specific											
Triangle	0.630	−0.193	0.577	−0.203	0.088	0.851	0.038	0.180	0.280	0.279	0.224
Orton1	0.029	0.217	0.023	0.202	0.007	0.293	0.221	2.335	0.101	0.097	0.106
Orton2	0.018	0.198	0.016	0.198	0.001	0.091	0.229	2.224	0.093	0.091	0.088
Orton3	0.004	0.048	0.003	0.051	0.000	0.015	0.105	1.535	0.110	0.110	0.083
Parker-A	0.006	0.117	0.006	0.119	0.000	0.029	0.164	1.742	0.097	0.097	0.084
Parker-S	0.014	0.184	0.012	0.183	0.001	0.068	0.219	2.269	0.093	0.093	0.087
Parker-E	0.013	0.170	0.011	0.171	0.001	0.058	0.202	2.155	0.092	0.091	0.086
Parker-T	0.012	0.164	0.011	0.165	0.000	0.055	0.255	1.881	0.092	0.091	0.085

K_{trans}, k_{ep}, k_{el} in $1/min$; v_p is a fraction; AH is in $1/min^2$; residual norm is in arbitrary units but it can be compared across all model combinations.

and group-specific AIF models. The exceptions were k_{ep} of Tofts and ETofts with Orton3, v_p of ETofts, and k_{ep} and k_{el} of Brix with Orton2, Orton3, and Parker, which were mostly found to have a higher CV for the group-specific AIF. When comparing the CV of the different models we noted that overall the CV for the Tofts' model was lower than the CV for the other models. Especially, the CV of K_{trans} was substantially larger in ETofts than Tofts. For ETofts, the CV of v_p was very high, demonstrating that the vascular component could not be precisely recovered, caused by the close to zero v_p (Table 4). The CV of the Brix model parameters was, overall, higher than the CV of the Tofts model parameters. The CV in patients (Table 7) was higher than in control subjects.

Discussion

This article presents a systematic comparative evaluation of AIF and pharmacokinetic models for quantitatively analyzing patellar perfusion with DCE-MRI.[19] Below, we derive several recommendations based on our results, and discuss the strengths, limitations, and impact.

The evaluation of digital phantom data shows that the proposed fitting method can accurately recover pharmacokinetic parameters when a correct AIF model is used. Although this phantom dataset simulates tumor perfusion,[24] which differs from patellar perfusion, the comparison with the ground truth confirms the technical validity of the proposed fitting methods.

TABLE 7. For Each AIF and Each Parameter of the Pharmacokinetic Models, the CV (%) Over the Five Patients

	Tofts		Extended Tofts			Brix			Residual		
	K_{trans}	k_{ep}	K_{trans}	k_{ep}	v_p	AH	k_{ep}	k_{el}	Tofts	ETofts	Brix
Literature-based											
Triangle	107.8	−40.6	108.9	−33.1	93.2	70.0	−409.6	50.2	46.4	46.2	25.4
Orton1	84.3	99.6	94.6	88.7	−120.9	85.1	18.0	58.8	25.6	24.8	23.2
Orton2	83.9	89.1	92.8	84.1	−175.4	89.3	76.4	31.4	24.5	24.2	23.2
Orton3	87.1	76.6	92.7	75.6	2356.5	87.1	29.9	49.4	22.7	23.0	22.3
Parker	91.2	86.5	94.1	83.3	359.9	85.4	24.5	68.0	24.0	24.1	22.6
Subject-specific											
Triangle	52.9	−40.5	71.2	−36.9	88.7	16.1	−199.9	67.1	83.7	83.5	80.8
Orton1	69.1	65.5	94.4	64.1	96.2	116.3	67.6	38.5	24.2	23.0	32.6
Orton2	100.9	71.9	119.3	70.9	140.8	128.4	75.7	72.4	20.7	20.4	25.4
Orton3	153.4	456.9	154.0	474.1	123.3	141.7	178.2	67.5	41.1	42.4	23.5
Parker-A	110.5	384.5	118.6	−9638.5	150.9	88.3	140.4	51.7	26.1	30.4	23.0
Parker-S	79.4	86.1	93.9	90.4	159.2	78.8	85.6	38.1	20.5	20.4	23.0
Parker-E	83.8	89.7	101.8	94.0	151.7	79.3	84.4	67.9	20.4	20.1	22.7
Parker-T	83.9	87.6	102.2	93.0	108.5	77.0	20.9	54.4	17.0	16.9	23.0
Group-specific											
Triangle	51.0	−39.5	64.0	−36.3	76.4	17.0	328.8	84.6	90.1	89.7	84.3
Orton1	74.0	54.1	94.5	53.5	80.5	119.4	54.0	28.5	24.2	23.2	31.7
Orton2	81.2	59.2	94.4	58.8	91.5	94.8	62.0	32.3	21.8	21.6	22.6
Orton3	91.2	175.7	96.0	165.3	−2921.1	78.2	114.0	41.3	26.4	26.8	22.5
Parker-A	87.4	83.2	94.9	81.8	107.7	82.9	77.2	57.1	21.8	22.0	22.6
Parker-S	82.7	61.9	94.6	61.9	72.8	90.8	63.6	35.6	21.5	21.6	22.4
Parker-E	83.8	64.0	95.1	64.0	81.9	88.8	66.1	39.6	21.3	21.4	21.8
Parker-T	84.4	65.5	94.1	65.5	70.9	88.1	82.3	57.9	21.2	21.4	21.9

The three right-most columns show the CV of the residual.

As indicated by the AIC scores, Triangle and Orton1 do not model the arterial signal well. For the Parker model, the increase in complexity from Parker-A to Parker-E is supported by the measured imaging data, since Parker-E leads to substantially improved arterial fits, reflected by lower AIC. This indicates that our addition of a persisting contrast concentration to the Parker-E model was justified. Overall, in terms of AIC, the most competitive models are Orton2, Parker-E, and Parker-T.

The AIC score shows substantially improved arterial fits of the subject and group-specific AIFs compared to the literature-based AIF. Moreover, except for Orton3, the literature-based AIFs lead to higher residuals when used in combination with the (E)Tofts pharmacokinetic model. Based on these results, we recommend against using a literature-based AIF.[27]

Since the large intersubject variability in the shape of the first-pass contrast concentration for subject-specific AIF modeling with Parker-E and Parker-T, and to a lesser extent with Orton2 and Orton3, cannot be explained biologically, similar to Ref. 28, the group-specific AIF is preferred for these models, despite the higher AIC value. Note that for Parker-E&T the CV of K_{trans} and AH is higher for the group-specific AIF than for the subject-specific AIF, while it is lower for k_{ep}. This suggests that components of the AIF relevant for determining K_{trans} can be recovered from an individual subject with a higher precision than the intersubject variation, whereas those components more relevant to determine k_{ep} cannot.

Comparing pharmacokinetic models, the CV typically is lowest for Tofts. This is probably due to the larger number of parameters in ETofts and Brix. The larger number of

parameters in Brix may also explain the 10% lower residual compared to Tofts. As all three pharmacokinetic models explain a similar fraction of the DCE-MRI signal, we expect that group differences, eg, between cases and controls, in perfusion cause similar relative changes in parameter values. This implies that the model with the smallest CV (Tofts) will likely be more sensitive to detect group differences than the other models (ETofts, Brix).

We chose to aggregate the voxel-wise pharmacokinetic measures by computing a weighted mean over the patella VOI. Any spatial heterogeneity within the patella is thus averaged out. Hence, it should be noted that using these measures to study group differences implicitly assumes non-localized physiological changes in the patella.

As no in vivo ground truth values for pharmacokinetic parameters are available, we could not base model selection on closeness to ground truth, and this implies that reliable absolute quantification of perfusion values currently cannot be claimed. As in Schmid et al,[17] we used a statistical analysis method to trade off model complexity against goodness-of-fit, in order to guide model selection. Note that, compared to Schmid et al, we evaluated a wider range of models, both for AIF and for pharmacokinetic model, and applied it to patellar DCE-MRI data.

The substantial differences in pharmacokinetic parameters obtained with different AIFs emphasize the relevance of choosing a good AIF model. Severe bias in parameters could occur with a suboptimal AIF. The small differences observed among the best candidates indicate that potentially other combinations can be best for acquisitions with different settings and/or in different body parts; even for other bones. Hence, our proposed framework for evaluating perfusion is an important contribution in itself. It allowed identification of a few combinations of AIF models and pharmacokinetic models that performed well in all aspects: AIC score and biological credibility of the AIF, CV of pharmacokinetic parameters, and goodness-of-fit in the patella VOI. Given the similarity in perfusion mechanisms and MR characteristics, we would expect these combinations to also perform well when studying perfusion in other bones such as tibia,[12] femur,[16] hip,[14] or bony pelvis.[15]

Although Orton2 combined with the Tofts' model seems to slightly improve reproducibility and goodness-of-fit in this dataset, we consider the lower AIC score of Parker-T as well as the improved biological credibility of that AIF to be more important. Together with the accuracy of this combination on phantom data, this gives good confidence that group-specific Parker-T combined with the Tofts' model is suitable to identify patellar perfusion abnormalities.

The observed values of the CV indicate that with a consistently used combination of models, reproducibility is sufficient to allow identification of group differences in perfusion with reasonably sized groups; eg, ~40 subjects per group allow identification of group differences of 10% in K_{trans} or k_{ep} at a significance level of $P < 0.05$ with 75% power.

In conclusion, the most suitable choice of models for the analyzed patellar DCE-MRI data is Parker's arterial input model, where all parameters of Parker's model are estimated from arterial voxels of the full group of subjects, combined with Tofts' pharmacokinetic model.

Acknowledgment

Contract grant sponsor: Hitachi Medical Systems/RSNA Research Seed Grant 2014; contract grant number: RSD1440
EUR fellowships: "Robust Quantitative MRI With Precision Estimates" and "Penetrating Patellofemoral Pain: A Cross-Sectional Case-Control Study."

References

1. Arnoldi CC, Lemperg RK, Linderholm H. Intraosseous hypertension and pain in the knee. J Bone Joint Surg Br 1975;57b:360–363.
2. Hejgaard N, Diemer H. Bone scan in the patellofemoral pain syndrome. Int Orthop 1987;11:29–33.
3. LaBrier K, O'Neill DB. Patellofemoral stress syndrome. Sport Med 1993;16:449–459.
4. Näslund JE, Odenbring S, Näslund U-B, Lundeberg T. Diffusely increased bone scintigraphic uptake in patellofemoral pain syndrome. Br J Sports Med 2005;39:162–165.
5. Näslund J, Waldén M, Lindberg L-G. Decreased pulsatile blood flow in the patella in patellofemoral pain syndrome. Am J Sports Med 2007;35:1668–1673.
6. Ho KY, Hu HH, Colletti PM, Powers CM. Recreational runners with patellofemoral pain exhibit elevated patella water content. Magn Reson Imaging 2014;32:965–968.
7. Lemperg RK, Arnoldi CC. The significance of intraosseous pressure in normal and diseased states with special reference to the intraosseous engorgement-pain syndrome. Clin Orthop Relat Res 1978;143–156.
8. Selfe J, Harper L, Pedersen I, Breen-Turner J, Waring J, Stevens D. Cold legs: A potential indicator of negative outcome in the rehabilitation of patients with patellofemoral pain syndrome. Knee 2003;10:139–143.
9. Dyke JP, Aaron RK. Noninvasive methods of measuring bone blood perfusion. Ann N Y Acad Sci 2010;1192:95–102.
10. Li SP, Padhani AR. Tumor response assessments with diffusion and perfusion MRI. J Magn Reson Imaging 2012;35:745–763.
11. Copen WA, Schaefer PW, Wu O. MR perfusion imaging in acute ischemic stroke. Neuroimaging Clin N Am 2011;21:259–283.
12. Seah S, Wheaton D, Li L, et al. The relationship of tibial bone perfusion to pain in knee osteoarthritis. Osteoarthr Cartil 2012;20:1527–1533.
13. Lee JH, Dyke JP, Ballon D, Ciombor DM, Rosenwasser MP, Aaron RK. Subchondral fluid dynamics in a model of osteoarthritis: use of dynamic contrast-enhanced magnetic resonance imaging. Osteoarthr Cartil 2009;17:1350–1355.
14. Lee JH, Dyke JP, Ballon D, Ciombor DM, Tung G, Aaron RK. Assessment of bone perfusion with contrast-enhanced magnetic resonance imaging. Orthop Clin North Am 2009;40:249–257.
15. Breault SR, Heye T, Bashir MR, et al. Quantitative dynamic contrast-enhanced MRI of pelvic and lumbar bone marrow: Effect of age and marrow fat content on pharmacokinetic parameter values. Am J Roentgenol 2013;200:297–303.
16. Budzik JF, Lefebvre G, Forzy G, El Rafei M, Chechin D, Cotten A. Study of proximal femoral bone perfusion with 3D T1 dynamic contrast-enhanced MRI: a feasibility study. Eur Radiol 2014;24:3217–3223.

17. Schmid VJ, Whitcher B, Yang G-Z, Taylor NJ, Padhani AR. Statistical analysis of pharmacokinetic models in dynamic contrast-enhanced magnetic resonance imaging. Med Image Comput Comput Assist Interv 2005;8(Pt 2):886–893.

18. Orton MR, d'Arcy JA, Walker-Samuel S, et al. Computationally efficient vascular input function models for quantitative kinetic modelling using DCE-MRI. Phys Med Biol 2008;53:1225–1239.

19. Parker GJM, Roberts C, Macdonald A, et al. Experimentally-derived functional form for a population-averaged high-temporal-resolution arterial input function for dynamic contrast-enhanced MRI. Magn Reson Med 2006;56:993–1000.

20. Tofts PS. Modeling tracer kinetics in dynamic. J Magn Reson Imaging 1997;7:91–101.

21. Van Der Heijden RA, Oei EHG, Bron EE, et al. No difference on quantitative magnetic resonance imaging in patellofemoral cartilage composition between patients with patellofemoral pain and healthy controls. Am J Sports Med 2016;44:1172–1178.

22. Bron EE, Van Tiel J, Smit H, et al. Image registration improves human knee cartilage T1 mapping with delayed gadolinium-enhanced MRI of cartilage (dGEMRIC). Eur Radiol 2013;23:246–252.

23. Brix G, Semmler W, Port RE, Schad L, Gunter L, Lorenz WJ. Pharmacokinetic parameters in CNS Gd-DTPA enhanced MR imaging. J Comput Assist Tomogr 1991;15:621–628.

24. Bosca RJ, Jackson EF. Creating an anthropomorphic digital MR phantom—an extensible tool for comparing and evaluating quantitative imaging algorithms. Phys Med Biol 2016;61:974.

25. Akaike H. A new look at the statistical model identification. IEEE Trans Autom Control 1974;19:716–723.

26. Ardekani BA, Kershaw J, Kashikura K, Kanno I. Activation detection in functional MRI using subspace modeling and maximum likelihood estimation. IEEE Trans Med Imaging 1999;18:101–114.

27. Fedorov A, Fluckiger J, Ayers GD, et al. A comparison of two methods for estimating DCE-MRI parameters via individual and cohort based AIFs in prostate cancer?: A step towards practical implementation. Magn Reson Imaging 2014;32:321–329.

28. Hormuth DA, Skinner JT, Does MD, Yankeelov TE. A comparison of individual and population-derived vascular input functions for quantitative DCE-MRI in rats. Magn Reson Imaging 2014;32:397–401.